

# Cholesterol Transport through Lysosome-Peroxisome Membrane Contacts

Bei-Bei Chu,<sup>1,2,3,5</sup> Ya-Cheng Liao,<sup>1,5</sup> Wei Qi,<sup>1</sup> Chang Xie,<sup>1</sup> Ximing Du,<sup>4</sup> Jiang Wang,<sup>3</sup> Hongyuan Yang,<sup>4</sup> Hong-Hua Miao,<sup>1</sup> Bo-Liang Li,<sup>1</sup> and Bao-Liang Song<sup>2,\*</sup>

<sup>1</sup>State Key Laboratory of Molecular Biology, Institute of Biochemistry and Cell Biology, Shanghai Institutes for Biological Sciences, Chinese Academy of Sciences, Shanghai 200031, China

<sup>2</sup>College of Life Sciences, the Institute for Advanced Studies, Wuhan University, Wuhan 430072, China

<sup>3</sup>College of Animal Sciences and Veterinary Medicine, Henan Agricultural University, Zhengzhou 450002, Henan Province, China

<sup>4</sup>School of Biotechnology and Biomolecular Sciences, University of New South Wales, Sydney, NSW 2052, Australia

<sup>5</sup>Co-first author

\*Correspondence: [blsong@whu.edu.cn](mailto:blsong@whu.edu.cn)

<http://dx.doi.org/10.1016/j.cell.2015.02.019>

## SUMMARY

Cholesterol is dynamically transported among organelles, which is essential for multiple cellular functions. However, the mechanism underlying intracellular cholesterol transport has remained largely unknown. We established an amphotericin B-based assay enabling a genome-wide shRNA screen for delayed LDL-cholesterol transport and identified 341 hits with particular enrichment of peroxisome genes, suggesting a previously unappreciated pathway for cholesterol transport. We show dynamic membrane contacts between peroxisome and lysosome, which are mediated by lysosomal Synaptotagmin VII binding to the lipid PI(4,5)P<sub>2</sub> on peroxisomal membrane. LDL-cholesterol enhances such contacts, and cholesterol is transported from lysosome to peroxisome. Disruption of critical peroxisome genes leads to cholesterol accumulation in lysosome. Together, these findings reveal an unexpected role of peroxisome in intracellular cholesterol transport. We further demonstrate massive cholesterol accumulation in human patient cells and mouse model of peroxisomal disorders, suggesting a contribution of abnormal cholesterol accumulation to these diseases.

## INTRODUCTION

Cholesterol, an essential lipid for eukaryotic cells, plays important roles in many cellular processes including membrane properties regulation, steroidogenesis, bile acid synthesis, and signal transduction. Accounting for ~30%–40% of total cellular lipids, cholesterol is dynamically transported in cells and unevenly distributed in cellular membrane structures. Only ~0.5%–1% of total cellular cholesterol is present in the ER membrane (Lange et al., 1999) and its concentration is higher in the Golgi apparatus and highest (~60%–80%) in the plasma membrane (PM) (Liscum and Munn, 1999). In addition, cholesterol exerts diverse cellular

functions in different organelles. Sterols in ER control de novo cholesterol biosynthesis by inhibiting SREBP processing and promoting degradation of HMG-CoA reductase (Goldstein et al., 2006). Cholesterol is esterified in ER for storage and lipoprotein secretion (Chang et al., 1997; Vance and Vance, 1990) and oxidized and converted to steroids and bile acids in mitochondria and peroxisome (Ishibashi et al., 1996). Thus, dynamic cholesterol transport in cells is pivotal for multiple cellular functions.

Low density lipoprotein (LDL)-derived cholesterol trafficking is a major part of intracellular cholesterol transport with most mammalian cells acquiring ~80% of their cholesterol through receptor-mediated endocytosis of plasma LDL (Brown and Goldstein, 1986). Upon receptor binding and internalization, LDL is delivered from early endosome to late endosome/lysosome (L/L), where LDL-derived cholesteryl esters are hydrolyzed to unesterified cholesterol. Free cholesterol then egresses from L/L and is further passed to downstream organelles such as the PM, ER, and mitochondria to fulfill its functions (Chang et al., 2006). To date, most mechanistic knowledge on cholesterol passage from L/L to other organelles has come from studies of the inheritable neuronal degeneration disorder Niemann Pick type C (NPC) disease, which is caused by loss-of-function mutations in *NPC1* or *NPC2* genes (Carstea et al., 1997; Sleat et al., 2004). NPC patients show severe cholesterol accumulation in multiple tissues. NPC1 is a polytopic membrane protein on L/L, whereas NPC2 is a luminal protein. After cholesteryl ester is hydrolyzed in the lysosomal lumen, NPC2 binds the unesterified cholesterol by recognizing the 8-carbon iso-octyl side chain. NPC2 then hands over the cholesterol molecule to the N-terminal domain of NPC1, with the 3 $\beta$ -hydroxyl group buried within the binding pocket. The NPC1-bound cholesterol projects through the glycocalyx and is inserted into the lysosomal membrane. In *NPC1* or *NPC2* mutant cells, cholesterol cannot be incorporated into membrane and is therefore accumulated in the lumen (Kwon et al., 2009). However, this only accounts for how free cholesterol reaches the L/L membrane, and the mechanisms whereby cholesterol leaves the lysosomal membrane and moves to other organelles remain largely unknown.

To identify critical proteins for intracellular cholesterol transport, we developed a cellular system using the antifungal

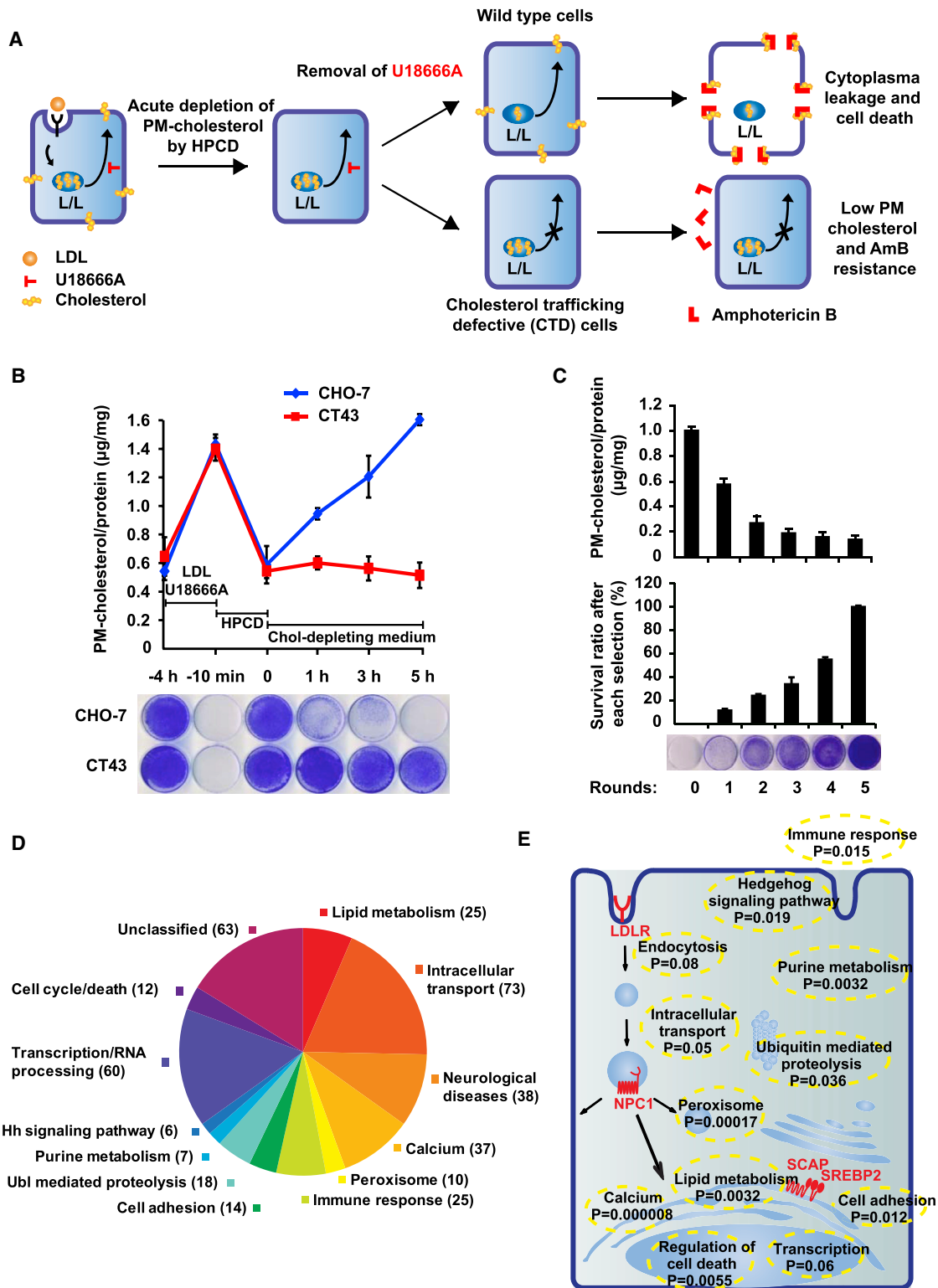


**Figure 1. Genome-wide RNAi Screen Identifies Genes Involved in Intracellular Cholesterol Transport**

(A) Schematic representation of the screen strategy.

(B) The cells were treated as shown in (A) and Figure S1C. The PM cholesterol and effect of AmB on cell growth at each time point were determined.

(C) PM cholesterol levels and survival ratio based on crystal violet staining of each selection round. Results represent the mean ± SD of three independent experiments.

(legend continued on next page)

antibiotic amphotericin B (AmB), in which cells only survive when they have impaired intracellular cholesterol transport. We performed a genome-wide pooled shRNA screen with the AmB system and identified over 300 genes affecting cholesterol transport. The genes encoding peroxisomal proteins were enriched. We further demonstrated that peroxisome forms transient lysosome-peroxisome membrane contact (LPMC) with lysosome through the binding of peroxisomal lipid PI(4,5)P<sub>2</sub> by lysosomal protein Synaptotagmin VII (Sy7). Cholesterol can be transported to peroxisome from lysosome through LPMC. Consistent with the latter findings, we observed drastic cholesterol accumulation in the X-chromosomal form of adrenoleukodystrophy (X-ALD) mouse model and in fibroblasts from human patients with different types of peroxisomal disorders. Our findings therefore reveal a fundamental role of peroxisome in intracellular cholesterol transport and suggest potential novel strategies for the diagnosis and treatment of peroxisome-related diseases.

## RESULTS

### Genome-wide Pooled shRNA Screening for Cholesterol Trafficking Defective Cells

AmB binds to cholesterol in PM and forms pores that lead to cytoplasm leakage and cell death (Andreoli, 1973). Based on this property, we designed a genome-wide shRNA screen to identify genes required for intracellular cholesterol transport, in particular the transport of cholesterol from LDL receptor (LDLR)-mediated endocytosis. The rationale and overall process of the screen are depicted in Figure 1A. There are three key elements, namely: (1) inhibition of endogenous cholesterol biogenesis throughout the entire process and delivery of cholesterol by LDL particles to focus on the transport of LDL-derived cholesterol, (2) synchronization of cells at the stage of high cholesterol in L/L and low cholesterol in PM so that the cholesterol can be transported to the PM in all cells at a given time point, and (3) enrichment of cholesterol trafficking defective (CTD) cells by using AmB that kills the cells with proper cholesterol transport in a controlled manner. The first key element is achieved by using lovastatin to inhibit HMG-CoA reductase and low concentration of mevalonate to only permit the synthesis of nonsterol isoprenoids essential for cell growth. Lipoprotein-deficient serum is also used before LDL delivery so that the cells are in cholesterol starvation and the initial LDLR level is very high. The second key element is realized by using U18666A, a compound that reversibly blocks cholesterol efflux from L/L (Liscum and Faust, 1989), and cyclodextrin, a cholesterol mobilizing reagent (Liu et al., 2010; Rosenbaum et al., 2010). Co-treatment of cholesterol-starved cells with LDL, lovastatin, and U18666A leads to LDLR-mediated endocytosis of large amounts of cholesterol which is trapped in L/L by U18666A. After a short exposure to cyclodextrin to acutely deplete cholesterol from PM, the cells are incubated without U18666A to allow cholesterol transport

from L/L to PM. AmB is then used to kill the cells with more cholesterol in PM. The cholesterol trafficking rate and PM-cholesterol level are lower in CTD cells than wild-type (WT) cells at particular time points. Thus, these CTD cells can survive AmB treatment.

The procedure described above was validated by comparing WT CHO-7- and *NPC1*-deficient CT43 cells (Figure 1B). Cyclodextrin decreased the PM-cholesterol level to 0.59 μg/mg protein. After removal of U18666A, PM-cholesterol level was much higher in CHO-7 than CT43 cells and the former was more sensitive to AmB treatment (Figure 1B). To perform the screen, HeLa cells were infected with a pooled shRNA library and the virus-infected cells were subjected to AmB selection as described above (Figure S1A). We observed gradual decrease of PM-cholesterol and increase of survival rate in the first five rounds of selection before reaching plateau (Figure 1C), suggesting that CTD cells were largely enriched. The shRNA inserts were then amplified from the CTD cells and subjected to deep sequencing.

The RNAi screening identified 341 candidate genes, each of which was targeted by two or more small hairpin RNAs (shRNAs), eliminating the off-target effect of shRNA. Their symbols and basic information are listed in Table S1.

### Analysis and Validation of Screening Results

To characterize the enriched biological processes and pathways in our screen, the 341 gene hits were subjected to gene ontology (GO) enrichment analysis and Kyoto Encyclopedia of Genes and Genomes (KEGG) database analysis (Figures 1D and 1E). The genes involved in lipid metabolism and intracellular transport were amply presented, constituting 28.7% of total candidates (Figures 1D and 1E). Among these hits, there is *NPC1*, loss of which is well known to trap cholesterol in lysosome and prevent cholesterol from traveling to PM. This serves as a positive control and suggests our screen was successful. Our screen also recovered genes that participate in *LDLR* expression regulation and endocytosis, such as *SREBP2*, *SCAP* (Brown and Goldstein, 1997), *LDLR* (Brown and Goldstein, 1986), and *AP2 associated kinase 1 (AAK1)* (Conner and Schmid, 2002). Because silencing of these genes prevents cells from taking up LDL, their appearance in the candidates list was expected.

Unexpectedly, we found marked enrichment for genes associated with neurological diseases, peroxisome, calcium, transcription/RNA processing, immune response, cell adhesion, Hh pathway, ubiquitin-mediated proteolysis, and purine metabolism. It is interesting that neurological disease-related genes are discovered in our screen to affect cholesterol transport. As exemplified by NPC disease, which is characterized by severe neurological symptoms secondary to cholesterol accumulation in lysosome, the neuron is particularly sensitive to cholesterol alteration, and impaired cholesterol transport may be a mechanism shared by these neurological diseases.

(D) Bioinformatics classification of the hits into biological processes and molecular functions categories. The number in the bracket shows the number of genes in each category.

(E) Statistically enriched biological processes superimposed on a sketch depicting a cell, with the corresponding p value of GO analysis in the screen. Genes in red refer to representative hits.

See also Figure S1 and Table S1.

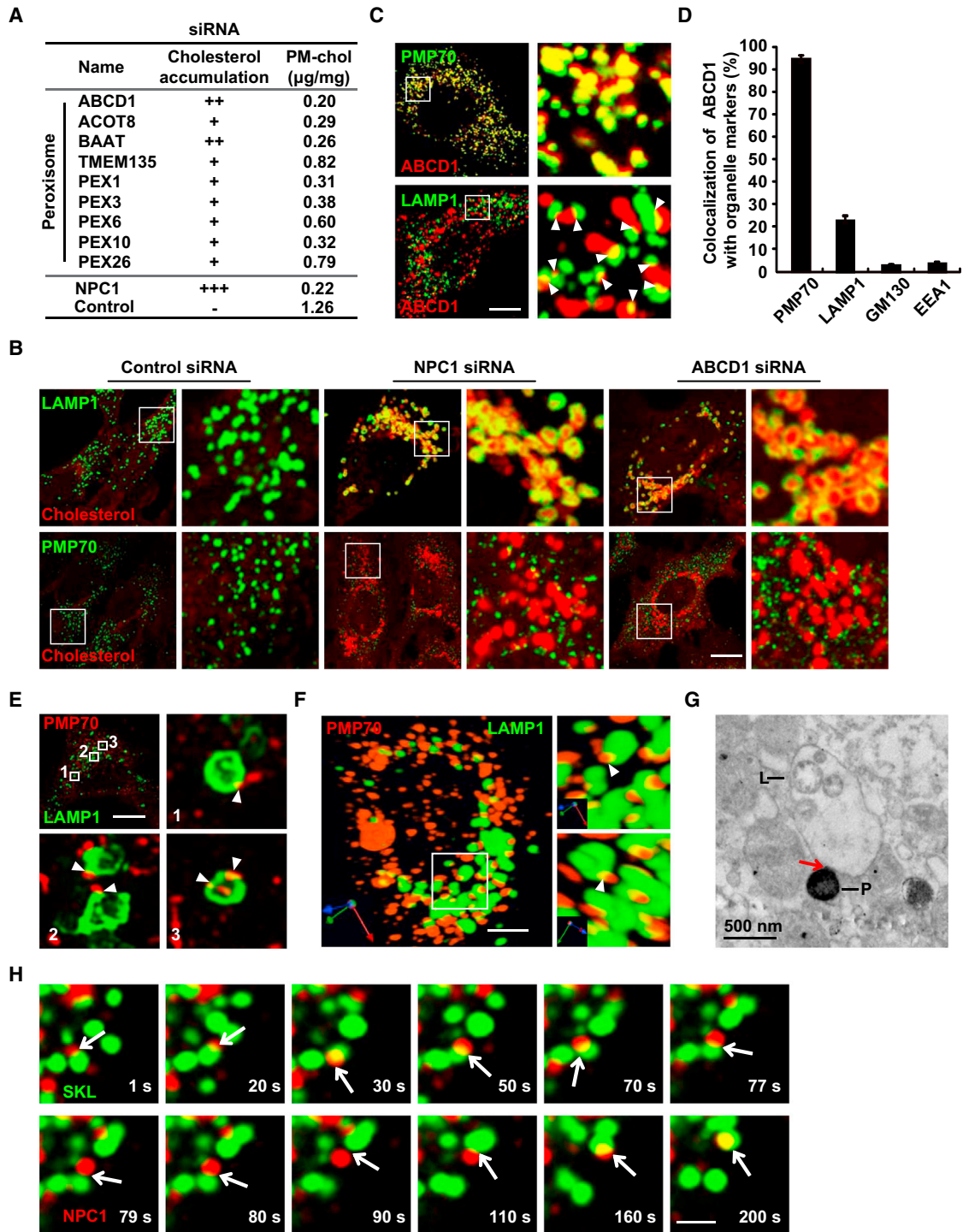


**Figure 2. Peroxisome Forms Transient and Dynamic Membrane Contacts with Lysosome**

(A) Knockdown of the peroxisome genes identified in the screen led to cholesterol accumulation and decrease of PM cholesterol levels. The “+” indicates the degree of cholesterol accumulation; the “-” indicates no obvious cholesterol accumulation.

(B) SV589 cells transfected with indicated siRNAs were stained with filipin (red) and antibody against endogenous LAMP1 (green) or PMP70 (green). Scale bar, 10 µm. LAMP1: lysosome marker, PMP70: peroxisome marker.

(C) HeLa cells transfected with mouse ABCD1-mCherry were assessed by immunostaining with antibody against PMP70 (green) or LAMP1 (green). Scale bar, 10 µm.

(D) Quantification of colocalization of ABCD1 with organelle-specific markers shown in (C) and Figure S3A. GM130, Golgi marker; EEA1, early endosome marker. Data represent mean ± SD (n = 4, 35 cells per independent experiment).

(legend continued on next page)

To further confirm the hits, we selected 30 representative genes covering all 14 classes and validated them using distinct shRNA sequences. The survival rate of knockdown cells is dramatically higher upon AmB treatment as compared with control cells (Figure S1D). Among the 30 representative genes, individual knockdown of 27 genes caused PM-cholesterol content to decrease by >50% (Figure S1F). Fifteen genes exhibited markedly enhanced cholesterol accumulation in cells as shown by filipin staining (Figure S1G). These results confirmed the reliability of our screen.

Intriguingly, genes encoding peroxisomal proteins were statistically enriched (Figures 1D and 1E). When the peroxisomal hits, including *ABCD1*, *ACOT8*, *BAAT*, *TMEM135*, *PEX1*, *PEX3*, *PEX6*, *PEX10*, and *PEX26* were individually knocked down, the PM-cholesterol level significantly decreased by 35%–84% as compared to control (Figure 2A). Cholesterol accumulation was observed in lysosome, but not peroxisome (Figures 2B and S2B).

### Peroxisome Forms Transient and Dynamic Contacts with Lysosome

How can depletion of peroxisomal proteins lead to cholesterol accumulation in lysosome? To answer this question, we used *ABCD1*, a peroxisomal membrane protein and also one of the strongest hits from our screen, as a representative to investigate the mechanism.

*ABCD1* mainly colocalized with the peroxisome marker PMP70 as expected. However, significant amount of colocalization between *ABCD1* and lysosome marker LAMP1 was surprisingly observed (Figures 2C, 2D, and S3A). Using GM130 as marker for the Golgi apparatus and EEA1 and Rab5 as early endosome markers, we found the lysosome-peroxisome contact was very specific as there was little detectable association between peroxisome and these two organelles (Figures 2D and S3A). Is the apparent colocalization of lysosome and peroxisome due to the sporadic distribution of *ABCD1* in lysosome? SKL is a strong peroxisome localization signal and the EGFP-His<sub>6</sub>-SKL protein is widely used to label peroxisome. We analyzed other peroxisome markers such as transfected EGFP-His<sub>6</sub>-SKL and endogenous PMP70 to rule out potential interference of particular marker or antibody and found a similar partial colocalization between lysosome and peroxisome (Figures S3A–S3C).

We took extra caution to further validate this phenomenon using 3D reconstitution, super resolution structured illumination microscopy (SR-SIM), and electron microscopy. 3D reconstitution and high resolution confocal images showed that the small membrane interaction between lysosome and peroxisome could indeed be observed using different microscopic methods (Figures 2E and 2F). Moreover, lysosome and peroxisome formed contacts in primary mouse hepatocytes detected by transmission electron microscopy (Figure 2G). With these validations, we named this phenomenon lysosome-peroxisome membrane

contact (LPMC). To our knowledge, the LPMC has not been reported before.

Time-lapse microscopy was next employed to understand the LPMC dynamics in living cells. It revealed that the contact between lysosome and peroxisome was only transient. In a time frame of a few dozen to 100 s, a particular peroxisome formed a contact with one lysosome, then was released and moved away. It could then associated with another lysosome in a similar time frame (Figure 2H; Movies S1 and S2). Notably, we observed no fusion of lysosome with peroxisome (Figure 2H). Consistently, a lysosomal matrix protein such as NPC2 was not detected in peroxisome when LPMC formed (Figure S3B).

To further validate the LPMC, we designed an organelle co-precipitation assay (Figure S3D). The cells stably expressing EGFP-His<sub>6</sub>-SKL were lysed without disturbing organelle integrity, and the membrane fractions were incubated with Ni Sepharoses to pull down peroxisome. The isolated fractions were then examined by fluorescent images of Ni Sepharoses and western blot. As shown in Figure S3E, NPC1-mCherry-labeled lysosome (red) could be observed on the beads covered by peroxisome (green). On the other hand, mCherry-Rab5-labeled early endosome was not co-precipitated suggesting the LPMC was specific. In line with these results, western blot analysis showed that the lysosomal protein LAMP1 was efficiently coprecipitated with peroxisome, but markers for other organelles were not (Figure S3F). Together, these lines of evidences strongly demonstrate the presence of LPMC.

We next examined if LPMC is regulated. Knockdown of *NPC1* or *ABCD1* significantly decreased the LPMC, with this effect being evident using both cell imaging and organelle co-precipitation methods (Figures 3A–3C). Depletion of other peroxisomal functional proteins such as *PEX1* also led to less LPMC (Figures S2B and S2C). More importantly, the LPMC was significantly reduced under cholesterol depletion status, and this reduction could be time-dependently reversed by cholesterol repletion from LDL (Figures 3D–3F). Knockdown of *LDLR*, *Clathrin heavy chain* (*CHC*), or co-depleting of adaptor proteins genes including *AP2 subunit alpha 2*, *ARH*, and *Dab2* to inhibit LDL endocytosis not only attenuated lysosomal cholesterol replenishment, but also decreased the LPMC (Figures 3G and 3H). These results suggest that cellular cholesterol content regulates LPMC, which also requires proper functions of lysosome and peroxisome.

### Synaptotagmin VII Is a Lysosomal Protein Binding Peroxisome

We next sought to identify the molecules bridging LPMC. A multi-arm proteomics approach was employed to analyze lysosomal membrane proteins, peroxisomal proteins, and NPC1 interacting proteins (Figures S4A and S4B; Table S2). After merging of the protein lists, candidates involved in vesicle fusion or organelle dynamics were selected as refined candidates for

(E) A representative SR-SIM image of the overlaid endogenous LAMP1 (green) and PMP70 (red) images. Arrowheads indicate LPMC sites. Scale bar, 10  $\mu$ m.

(F) HeLa cells were immunostained with antibodies against LAMP1 and PMP70 and analyzed by Volocity-3D software. Arrowheads indicate LPMC sites. Scale bar, 10  $\mu$ m.

(G) Transmission electron micrograph of the LPMC in a mouse liver cell. L, lysosome, P, peroxisome. Scale bar, 500 nm.

(H) SV589 cells were transfected with EGFP-SKL and NPC1-mCherry. Time-lapse images were acquired. Scale bar, 500 nm. See also Movie S2.

See also Figures S2 and S3 and Movies S1 and S2.

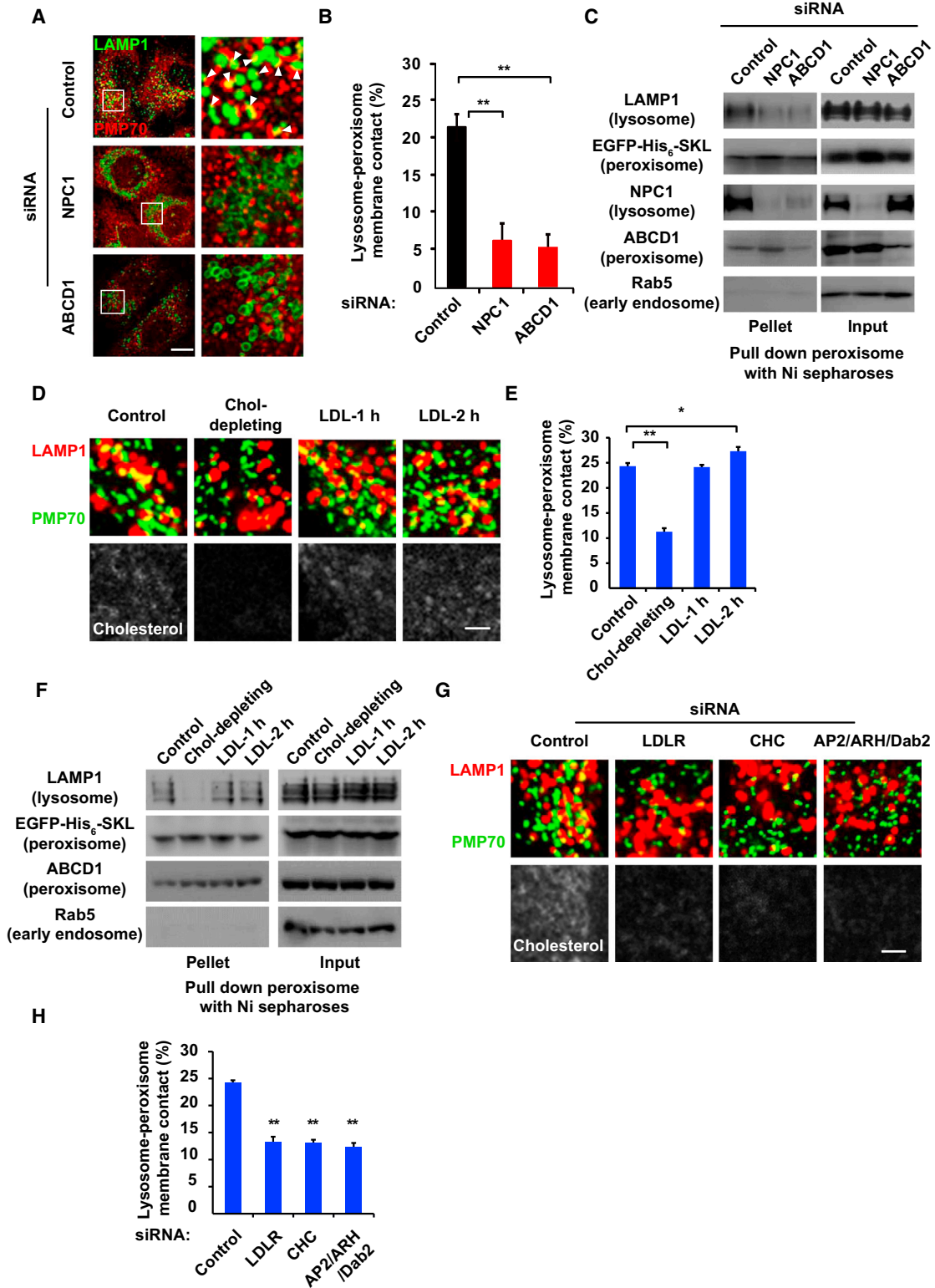


**Figure 3. Regulation of Lysosome-Peroxisome Membrane Contacts**

(A) SV589 cells were transfected with indicated siRNAs and immunostained with antibodies against LAMP1 (green) and PMP70 (red). Scale bar, 10  $\mu$ m.

(B) Quantification of LPMC in (A). Data represent mean  $\pm$  SD. \*\* $p < 0.01$ , one-way ANOVA ( $n = 4, 35$  cells per independent experiment).

(C) Lysosome-peroxisome association revealed by organelle co-precipitation assay.

(legend continued on next page)

RNAi validation (Table S2). Out of the 16 candidates, Synaptotagmin VII (Syt7) was the only that passed the validation: its knockdown but not that of others caused clear cholesterol accumulation in cells (Figure S4C).

Synaptotagmin is a family of proteins involving in vesicle interaction and fusion. Syt7 is widely expressed and plays important role in lysosomal exocytosis, membrane resealing, and wound healing (Andrews and Chakrabarti, 2005). Syt7 mainly colocalized with the lysosome marker LAMP1 (Figure 4A). Similarly to NPC1 and LAMP1, Syt7 significantly colocalized with the peroxisome marker PMP70 but not markers for Golgi or early endosome (Figures 4A and 4B). Knockdown of Syt7 resulted in cholesterol accumulation in lysosome (Figure 4C), and the LPMC was also dramatically diminished (Figure 4D). Syt7 is a transmembrane protein with a short N-terminal ectodomain, a single transmembrane segment, and a large cytosolic region containing two tandem  $\text{Ca}^{2+}$ -binding C2 domains (C2A and C2B, Figure 4E). The C2A and C2B domains are responsible for the  $\text{Ca}^{2+}$ -dependent interactions between Syt7 and SNAREs or phospholipids. When overexpressed, these domains compete for binding to SNAREs or phospholipids and function as dominant-negative forms (Desai et al., 2000). We utilized a similar method and found that overexpression of C2A or C2B domain dramatically inhibited LPMC in cell imaging and organelle coimmunoprecipitation (coIP) (Figures 4F, 4G, and S4D), accompanied by cholesterol accumulation in cells (Figure 4H).

We further developed an *in vitro* reconstitution assay to dissect the mechanism of LPMC (Figure S5A). Briefly, EGFP-His<sub>6</sub>-SKL-labeled peroxisome and NPC1-FLAG-mCherry-labeled lysosome were separately isolated by density gradient centrifugation. The peroxisomes were further precipitated by Ni Sepharoses and incubated with purified lysosome fractions. After incubation, Ni Sepharoses were separated by centrifugation and subjected to confocal microscopy and western blot. As shown in Figure S5B, lysosome labeled as red was pulled down with peroxisome in the presence of cytosol and ATP/GTP. Consistently, the lysosome marker NPC1-FLAG-mCherry was co-precipitated at this condition (Figure 4I). These results suggest energy and some cytosolic proteins may facilitate LPMC. Addition of dominant-negative Syt7-C2AB protein (Figure S5C) in the incubation step blocked the lysosome peroxisome interaction (Figures 4J and S5D). Similarly, when lysosomes from Syt7 or NPC1 RNAi-depleted cells were incubated with control peroxisome, the LPMC was significantly reduced. Conversely, when lysosome from control cells was incubated with peroxisome from Syt7 or NPC1 RNAi-depleted cells, the LPMC was not affected (Figures 4K and S5E). These findings indicate Syt7 is a lysosomal protein required for LPMC formation.

### PI(4,5)P<sub>2</sub> in Peroxisome Membrane Bridges LPMC

It has been documented that SNAREs mediate membrane contacts and fusion throughout the secretory pathway (Chen and Scheller, 2001; Weber et al., 1998). Organelles such as Golgi, ER, and lysosome are all maintained by SNARE-based fusion events. However, so far, no peroxisomal SNARE protein has been identified. Consistent with previous studies (Matsumoto et al., 2003), no SNARE family protein was identified in our peroxisomal proteomics (Table S2). Because Syt7 binds to phospholipids besides SNARE, we hypothesized that Syt7-mediated LPMC might be through its interaction with peroxisomal phospholipids. To test this hypothesis, we examined the binding specificity of Syt7-C2AB to various phospholipids in a PIP-strip assay. Syt7-C2AB mainly bound PI(4,5)P<sub>2</sub> and to a much lesser extent PI(5)P and PS; no signal was observed for other phospholipids (Figure 5A). It has been reported that peroxisome can synthesize significant amounts of PIP<sub>2</sub> including PI(4,5)P<sub>2</sub> (Jeynov et al., 2006). To further validate Syt7-PI(4,5)P<sub>2</sub> interaction under a more relevant format, we performed the liposome flotation assay using liposomes mimicking phospholipid composition of the mammalian peroxisome membrane (PC:PE:PI:PS = 54:36:5:5) (Hardeman et al., 1990). As shown in Figure 5B, when mixed with blank liposomes or PI5P containing liposomes, the His<sub>6</sub>-C2AB protein was predominantly detected in the bottom fraction. Trace amount of His<sub>6</sub>-C2AB in middle and top fractions was also detected, possible due to the weak binding of C2AB to PS and PI5P. In contrast, the majority of His<sub>6</sub>-C2AB protein was co-floated with liposomes containing PI(4,5)P<sub>2</sub> to the top fraction. These results demonstrated that the C2AB domain of Syt7 interacts with PI(4,5)P<sub>2</sub> in membrane.

Next, we sought to determine whether the Syt7-PI(4,5)P<sub>2</sub> interaction functions to bridge LPMC using an inducible FKBP12-FRB heterodimerization system to deplete PI(4,5)P<sub>2</sub> on peroxisome (Figure 5C). In the constructed SV589 cells, FKBP12 was targeted to peroxisome by fusion with PEX-mCherry, and the inositol polyphosphate 5-phosphatase synaptojanin 2 (SYNJ2) was kept in cytoplasm fused with mCitrine-FRB. Application of the chemical inducer rapamycin led to peroxisome membrane recruitment of mCitrine-FRB-SYNJ2 by binding PEX-mCherry-FKBP12 (Kapitein et al., 2010), which rapidly and irreversibly converted PI(4,5)P<sub>2</sub> to PI(4)P (Figures 5C and 5D). As shown in Figures 5E and 5F, rapamycin treatment caused a significant decrease of LPMC and cellular cholesterol accumulation. The cell expressing only mCitrine-FRB was a control showing no change of LPMC or cholesterol aggregation. Although cellular PI(4,5)P<sub>2</sub> also presents on PM, depletion of PI(4,5)P<sub>2</sub> in PM by a similar strategy did not decrease LPMC or cause cholesterol accumulation (Figures S6A–S6C). Furthermore, anti-PI(4,5)P<sub>2</sub> antibody specifically reduced the association between lysosome and peroxisome *in vitro* (Figures 5G, 5H, and S5F). Together,

(D) HeLa cells were incubated in cholesterol-depleting medium for 16 hr and then refed with LDL for different time durations. Cells were stained with filipin (gray) and antibodies against LAMP1 (red) and PMP70 (green). Scale bar, 2  $\mu\text{m}$ .

(E) Quantification of LPMC in (D). Data represent mean  $\pm$  SD (n = 4, 35 cells per independent experiment). \*\*p < 0.01, \*p < 0.05.

(F) Organelle co-precipitation assay was performed to validate LPMC when cells were grown under conditions shown in (D).

(G) SV589 cells transfected with indicated siRNAs were stained with filipin (gray) and antibodies against LAMP1 (red) and PMP70 (green). Scale bar, 2  $\mu\text{m}$ .

(H) Quantification of LPMC in (G). Data represent mean  $\pm$  SD (n = 4, 35 cells per independent experiment). \*\*p < 0.01.

See also Figure S3.

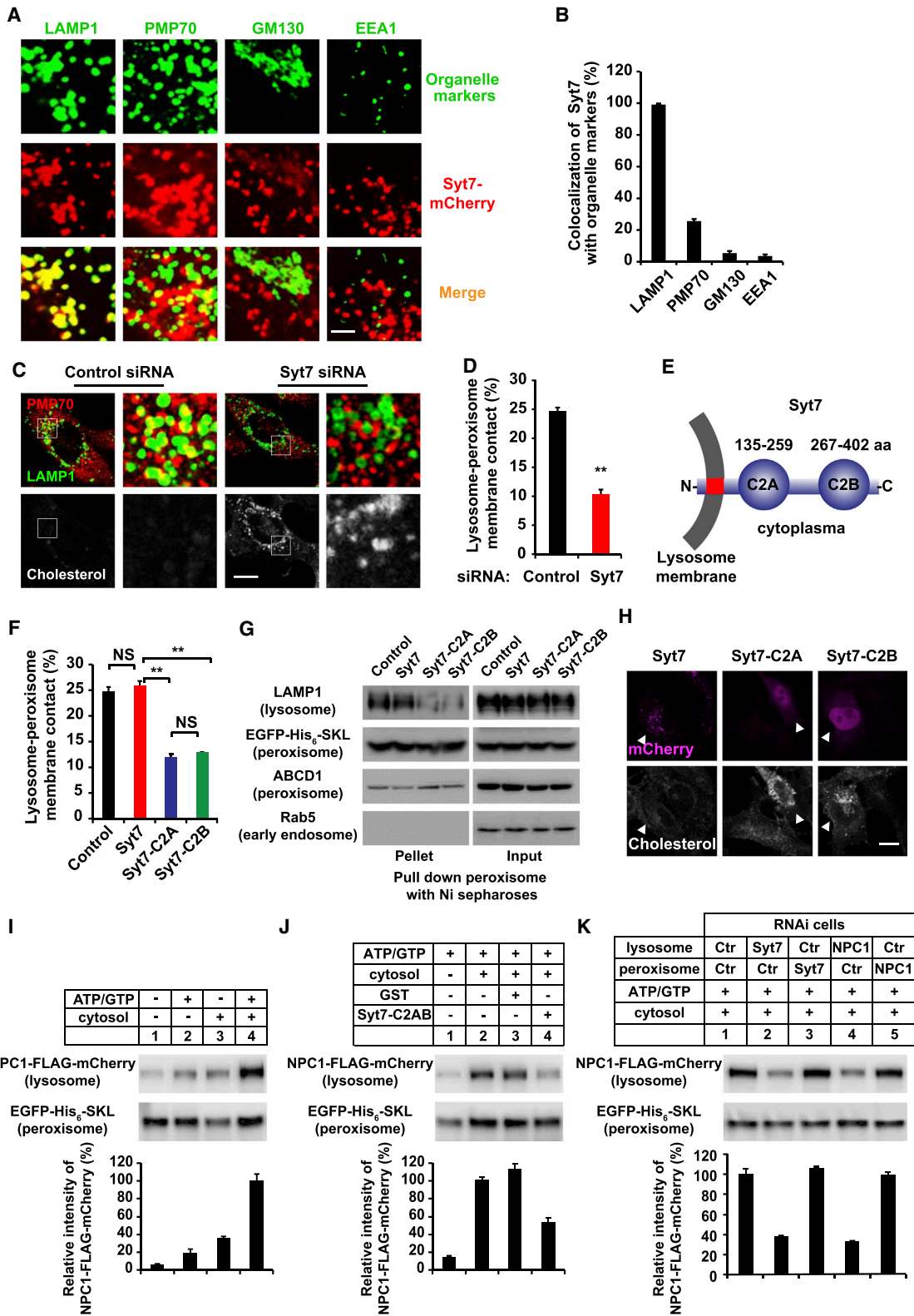


**Figure 4. Synaptotagmin VII Is a Lysosomal Protein Bridging LPMC**

(A) SV589 cells transfected with Syt7-mCherry were assessed by immunostaining with indicated antibodies. Scale bar, 2 μm.

(B) Quantification of Syt7 colocalization with organelle-specific markers. Data represent mean ± SD (n = 4, 35 cells per independent experiment).

(legend continued on next page)

these data demonstrate that PI(4,5)P<sub>2</sub> in peroxisome membrane is required for LPMC and proper cholesterol transport.

Because PI(4,5)P<sub>2</sub> is critical for LPMC, we reasoned that the peroxisome genes from our screen might affect peroxisomal PI(4,5)P<sub>2</sub> level either directly or indirectly. Indeed, a pronounced decrease in the amount of PI(4,5)P<sub>2</sub> in peroxisomal lipid extraction was detected using dot blots with anti-PI(4,5)P<sub>2</sub> antibody after knocking down *ABCD1* or other peroxisomal hits (Figure S6D). These data suggest that the nine peroxisome proteins may not directly bind Syt7 but rather influence peroxisomal PI(4,5)P<sub>2</sub> level thereby affecting lysosome association.

### Cholesterol Transport through LPMC

To monitor cholesterol transport directly, we used <sup>3</sup>H-cholesterol in the in vitro reconstitution assay (Figure 6A). Briefly, <sup>3</sup>H-cholesterol-labeled lysosome was isolated by density centrifugation from HEK293T cell pre-incubated with <sup>3</sup>H-cholesterol. Peroxisome was purified from unlabeled cells. The lysosome and peroxisome were then applied to the in vitro reconstitution system. After incubation, EGTA washing was performed to dissociate lysosome from peroxisome while leaving the peroxisome on Ni Sepharoses. The <sup>3</sup>H-cholesterol in peroxisome was then measured. To control the specificity, antibodies against PI(4,5)P<sub>2</sub> or unrelated IgG were applied. The <sup>3</sup>H-cholesterol in peroxisome increased in a time-dependent manner and this increase was blocked by anti-PI(4,5)P<sub>2</sub> antibody (Figures 6B and S7A). In addition, lysosomes prepared from *NPC1* or *Syt7* RNAi cells failed to support cholesterol transfer to peroxisome (Figure 6C), because LPMC did not form when *NPC1* or *Syt7* was depleted from lysosome (Figures 4K and S5E). These data demonstrate that cholesterol can transfer from lysosome to peroxisome depending on LPMC in vitro.

What about in cells? We performed confocal microscopy on HeLa cells refed with LDL and observed a time-dependent increase of co-localization between peroxisome and cholesterol (Figures S7B and S7C). We also directly measured the cholesterol level in isolated lysosome and peroxisome after incubation with <sup>3</sup>H-cholesteryl oleate containing LDL (scheme in Figure S7D). The lysosome and peroxisome were both labeled by <sup>3</sup>H-cholesterol although peroxisome label was less (Figure 6D). Results from western blot of organelle markers excluded the contamination with other organelles (Figure S7E). Furthermore,

knockdown of *NPC1* or *ABCD1* caused significant increase of <sup>3</sup>H-cholesterol in lysosome and decrease in peroxisome (Figure 6D). LDL pulse chase experiment (Figure S7F) followed by SR-SIM microscopy showed that there was overlay of peroxisome with cholesterol-loaded lysosome, or cholesterol (Figure S7G). These data suggest cholesterol flows from lysosome to peroxisome in cells.

To further investigate whether LPMC is required for LDL-cholesterol transport to the ER, we performed SREBP cleavage and cholesterol esterification assays because it is well established that cholesterol derived from LDL prevents SREBP processing and stimulates cholesterol esterification once it reaches the ER. The results showed that LDL-cholesterol could efficiently block SREBP processing (Figure 6E) and stimulate cholesterol esterification (Figure 6F) in control cells. However, these effects were markedly blunted in *NPC1*, *ABCD1*, or *Syt7* RNAi cells (Figures 6E and 6F); demonstrating that cholesterol transport to ER was largely impaired when LPMC was disrupted.

With the current data and information from previous reports (Kwon et al., 2009), we propose the below model for cholesterol transport from lysosome to peroxisome. After internalization, LDL particles are delivered to lysosome where LDL-containing cholesteryl ester is hydrolyzed to unesterified cholesterol. The luminal NPC2 protein binds free cholesterol with the 8-carbon isoctyl side chain buried within the binding pocket and hands over the cholesterol molecule to the N-terminal domain of NPC1. The NPC1-N-terminal domain can penetrate the glycocalyx and facilitate cholesterol to insert into the lysosomal membrane. Lysosome and peroxisome form close membrane contacts through interaction between Syt7 and PI(4,5)P<sub>2</sub>. Thus, cholesterol can move from lysosome to peroxisome (Figure 6G).

### Intracellular Cholesterol Accumulation in Peroxisomal Disorders

*ABCD1* mutation causes X-ALD, which is a neurological disease with progressive CNS demyelination and adrenal insufficiency (Forss-Petter et al., 1997). X-ALD is one of the prevalent peroxisomal disorders and there is no effective treatment (Moser et al., 2005). Our work has demonstrated cholesterol transports from lysosome to peroxisome through LPMC, and *ABCD1* depletion impairs LPMC and leads to cholesterol accumulation. However, there is no previous report on cholesterol transport defect in

(C) SV589 cells transfected with indicated siRNAs were stained with filipin (gray) and antibodies against LAMP1 (green) and PMP70 (red). Insets show high magnification of the areas framed by a white box. Scale bar, 10 μm.

(D) Quantification of LPMC in (C). Data represent mean ± SD (n = 4, 35 cells per independent experiment). \*\*p < 0.01.

(E) Domain structure of the Syt7 protein.

(F) SV589 cells transfected with mCherry, Syt7, C2A, or C2B of Syt7 were assessed by immunostaining with antibodies against LAMP1 and PMP70. Shown is the quantification of LPMC. Data represent mean ± SD (n = 4, 30 cells per independent experiment). NS, not significant, \*\*p < 0.01. The fluorescence images of cells are shown in Figure S4D.

(G) HeLa/EGFP-His<sub>6</sub>-SKL cells were transfected with the indicated plasmids and the lysosome-peroxisome association was analyzed by organelle co-precipitation assay.

(H) SV589 cells transfected with the indicated plasmids were stained with filipin (gray). Arrowheads indicate the cells expressing Syt7 or Syt7 variants (magenta). Scale bar, 10 μm.

(I) In vitro reconstitution of LPMC. The images of Ni Sepharoses are shown in Figure S5B.

(J) Recombinant GST or Syt7-C2AB protein was applied in the in vitro reconstitution system. The images of Ni Sepharoses are shown in Figure S5D.

(K) Lysosome or peroxisome was purified from cells transfected with indicated siRNAs and then used for the in vitro reconstitution assay. The images of Ni Sepharoses are shown in Figure S5E. Ctr, control.

See also Figures S4 and S5 and Table S2.

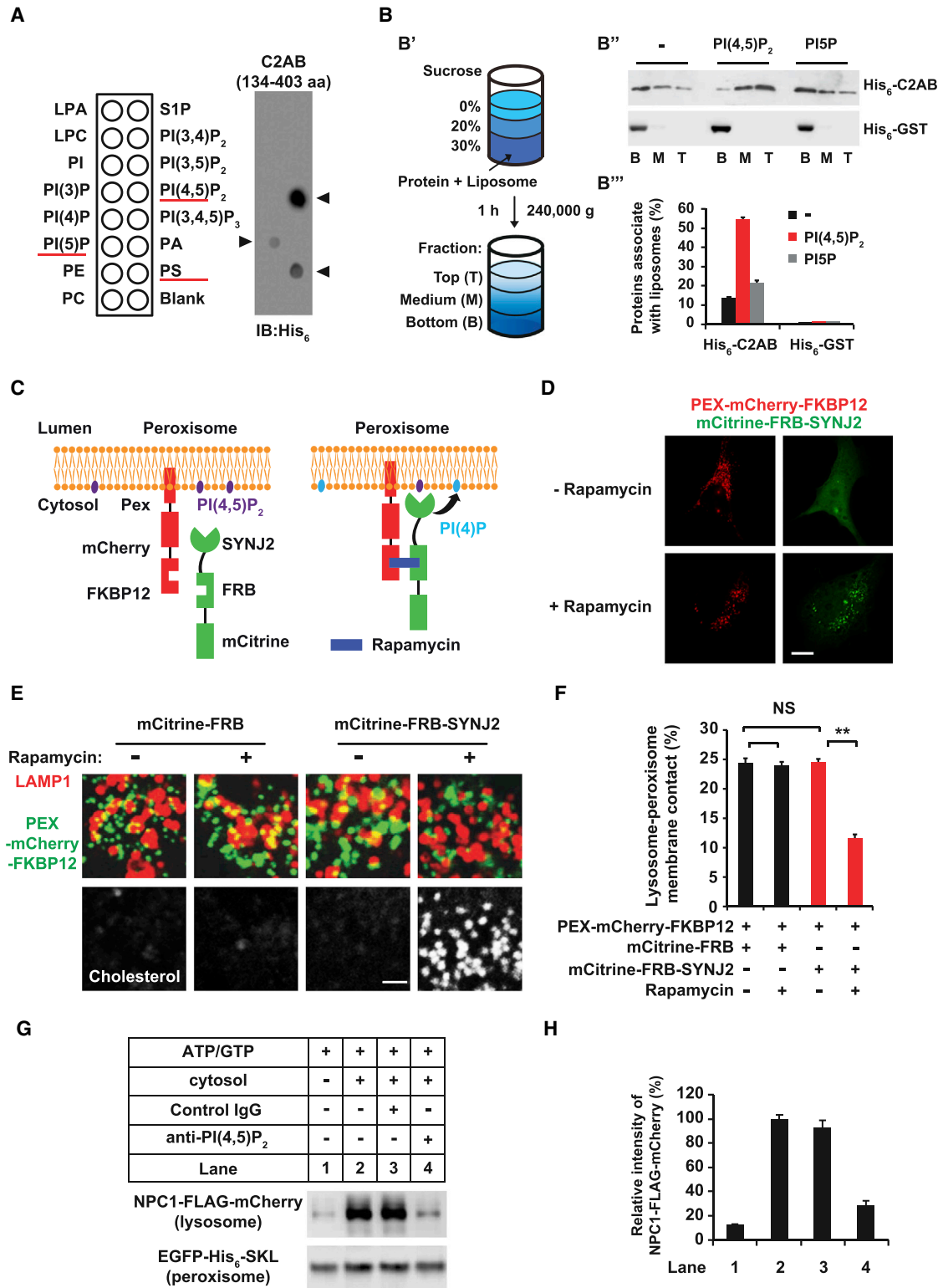


**Figure 5. PI(4,5)P<sub>2</sub> of Peroxisome Is Required for LPMC**

(A) Protein-lipid overlay. A scheme of the PIP-strip membrane is shown (left). Arrowheads indicate specific lipids binding. Red lines highlight the phospholipid species.

(legend continued on next page)

X-ALD or any other peroxisomal disorders. Therefore, we sought to validate our findings in vivo by examining if there is cholesterol accumulation in *ABCD1* knockout (KO) animal models and fibroblasts of human patients with different types of peroxisomal disorders.

As shown in Figure 7A, cholesterol accumulated in zebrafish embryo cells injected with morpholino antisense oligomer (MO) against *NPC1* or *ABCD1*. Furthermore, cholesterol accumulation was observed in fibroblasts, cerebellum, and adrenal gland of *ABCD1* KO mice (Figures 7B and 7C), a well-accepted animal model capturing the pathological characteristics of X-ALD. Interestingly, in the adrenal gland cholesterol deposits were located almost exclusively in the cortex but not in the medulla (Figure 7C), correlating with *ABCD1*'s specific expression in the cortex (Troffer-Charlier et al., 1998).

Because it is known that the *ABCD1* KO mice do not show an abnormal behavioral or neurological phenotype up to 15 months, we analyzed the behavioral deficits associated with CNS demyelination using rotarod test at the age of 7 and 20 months, respectively. When compared with WT littermates, the 20-month-old *ABCD1* KO mice displayed a marked impairment (19%) in their ability to stay on top of a rotated cylinder during 2 days trial, while the 7-month-old *ABCD1* KO mice were not affected (Figure 7D). Open field mobility paradigm was also used to study spontaneous locomotion and exploratory behavior. As shown in Figures 7E and 7F, the 20-month-old *ABCD1* KO mice exhibited significantly fewer numbers of rearings and traveled shorter distances in comparison with WT mice or 7-month-old *ABCD1* KO mice. This is important because the cholesterol accumulation occurs as early as 7 months (Figure 7C), long before the manifestation of the neurological phenotypes (20-month-old), suggesting not only that losing of *ABCD1* leads to cholesterol trafficking defects, but also that intracellular cholesterol accumulation might be a mechanism causing X-ALD symptoms.

To further evaluate the role of peroxisome in cholesterol trafficking, cultured fibroblasts from patients with X-ALD, or two peroxisome biogenesis disorders Infantile Refsum disease (IRD) and Zellweger syndrome (ZS) were used for cholesterol staining. As shown in Figure 7G, drastic cholesterol accumulation was observed in these fibroblasts, suggesting peroxisome plays an essential role in intracellular cholesterol transport.

## DISCUSSION

Using an elegantly designed cellular system, our genome-wide shRNA screen allows a comprehensive dissection of the genes

and pathways that may regulate intracellular cholesterol transport. Besides the previously known cholesterol transport gene like *NPC1*, we uncovered over 300 additional genes, among which the genes encoding peroxisomal proteins were highly enriched.

We showed that peroxisome played an essential role in intracellular cholesterol transport through forming membrane contacts with lysosome. We provided multiple lines of evidence to solidify this observation. First, LPMC was observed by confocal microscopy and decreased by cholesterol depletion and knocking down of *NPC1* or *ABCD1*. Second, super resolution microscopy showed the overlapping signals between peroxisome and lysosome (Figure 2E). Third, 3D reconstitution verified LPMC from different angles (Figure 2F). Fourth, transmission electron micrographs directly observed LPMC in primary mouse hepatocytes (Figure 2G). Fifth, time-lapse imaging showed the LPMC is dynamic in living cells (Figure 2H). Sixth, organelle coprecipitation assay detected the physical interaction between peroxisomes and lysosomes (Figures 3C and S3F). Seventh, in vitro reconstitution assay confirmed that lysosome and peroxisome can form contacts specifically (Figures 4I and S5).

As for the molecules bridging LPMC, our data demonstrate lysosomal protein Syt7 binds peroxisomal lipid PI(4,5)P<sub>2</sub> to form a transient contact. How are Syt7 activation and peroxisomal PI(4,5)P<sub>2</sub> level regulated? It is well known that calcium can bind Syt7 leading to a conformational change (Fukuda and Mikoshiba, 2001). Meanwhile, the level of PI(4,5)P<sub>2</sub> can be modulated by phosphatidylinositol kinases and phosphatases. Its distribution is also under dynamic regulation. Therefore, how different proteins/pathways regulate Syt7 and PI(4,5)P<sub>2</sub> and then influence LPMC and cholesterol transport is a particular interesting subject for further exploration. The in vitro reconstitution assay developed in this study would be a powerful tool. Our screen discovered 9 peroxisomal proteins including *ABCD1*, knockdown of which individually leads to lowered peroxisomal PI(4,5)P<sub>2</sub> level (Figure S6D). These nine peroxisomal proteins cover different functions and are all required for proper peroxisomal function. Therefore, the dysfunction of peroxisome may underlie the decrease of PI(4,5)P<sub>2</sub> and LPMC. Further studies are still needed to understand how these peroxisome proteins are functionally connected to PI(4,5)P<sub>2</sub> regulation.

Previous studies have indicated that cholesterol can leave lysosome by vesicular or non-vesicular transport. Urano et al. (2008) showed that LDL-cholesterol can be transported from L/L to the trans-Golgi network through vesicular trafficking. Du et al. (2011) reported that ORP5, an oxysterol-binding protein-related

(B) B': workflow of the liposome flotation assay. B'': the presence of recombinant proteins in the top (T), middle (M), and bottom (B) fractions were detected by western blot using anti-His<sub>6</sub> antibody. B''': semiquantitative densitometric analysis of western blot in B''. The amount of liposomes-associated proteins was determined by comparing proteins present in the top fraction to the total amount of proteins present in the top, middle, and bottom fractions.

(C) Schematic representation of the rapamycin-inducible heterodimerization system used to recruit SYNJ2 to the peroxisome membrane.

(D) Validation of the rapamycin-inducible system in SV589 cells. Scale bar, 10 μm.

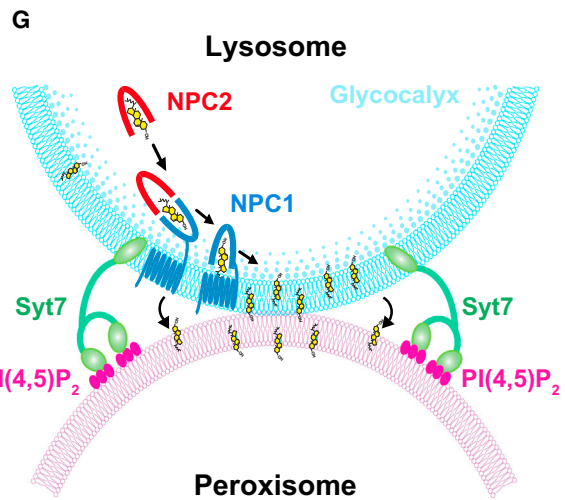
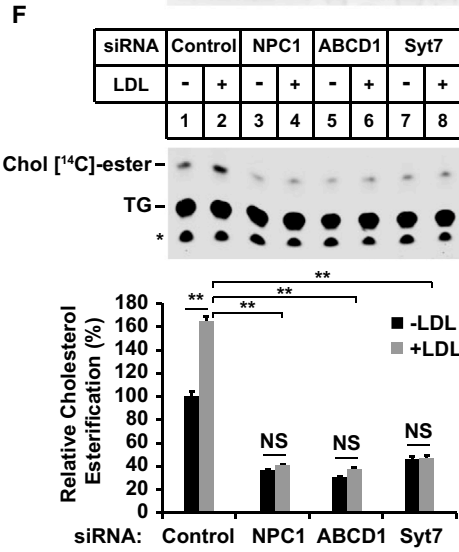
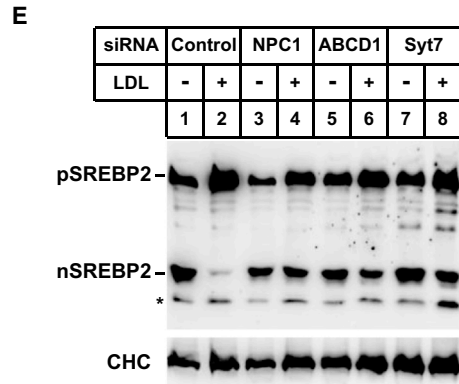
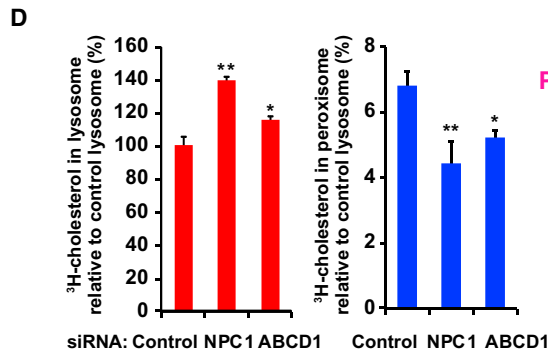
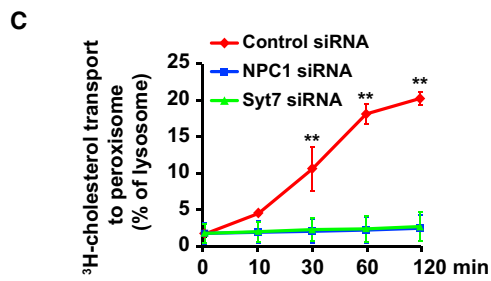
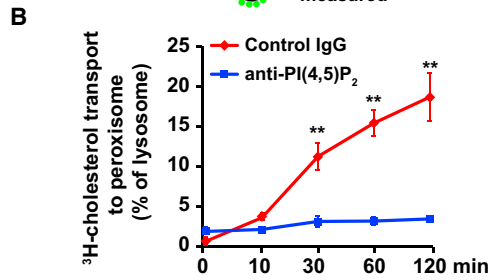
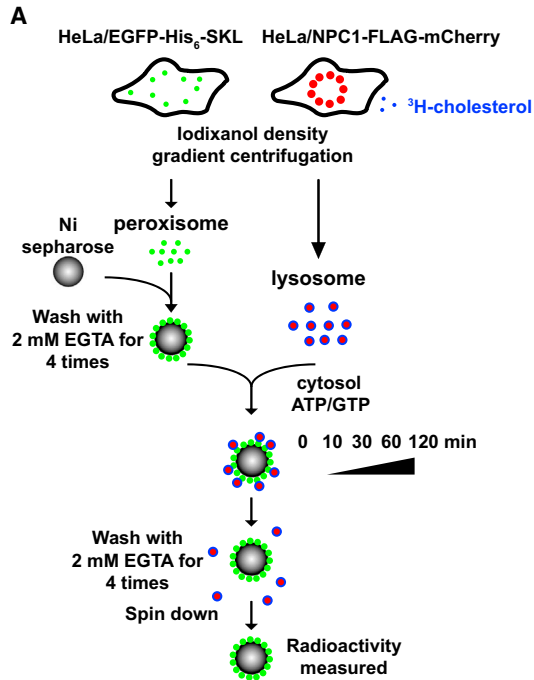
(E) SV589 cells were transfected with PEX-mCherry-FKBP12 together with either mCitrine-FRB or mCitrine-FRB-SYNJ2. Cells were then treated with rapamycin, stained with filipin (gray), and immunostained with antibody against LAMP1, followed by Cy5-conjugated anti-mouse secondary antibody (pseudocolor, red). Scale bar, 2 μm.

(F) Quantification of LPMC in (E). Data represent mean ± SD (n = 4, 30 cells per independent experiment). NS, not significant, \*\*p < 0.01.

(G) Anti-PI(4,5)P<sub>2</sub> or control IgG was applied in the in vitro reconstitution system. The images of Ni Sepharoses are shown in Figure S5F.

(H) Semiquantitative densitometric analyses of (G).

See also Figures S5 and S6.



(legend on next page)

protein, may mediate cholesterol efflux from lysosome to ER through binding cholesterol and NPC1. Here, cholesterol transport across LPMC is another mechanism for cholesterol efflux from lysosome. Disruption of LPMC by different means causes significant lysosomal cholesterol accumulation. X-ALD animal models and fibroblasts of human patients with different types of peroxisomal disorders displayed drastic cholesterol accumulation (Figure 7), suggesting LPMC is a major route for cholesterol to leave the lysosomal membrane. Our in vitro reconstitution assay suggests cytosol may facilitate cholesterol movement from lysosome to peroxisome (Figure 4I). Finally, it is possible that cytosolic cholesterol binding proteins such as StarD4 and ORPs may accelerate the cholesterol movement from lysosomal membrane to peroxisome when LPMC forms.

After reaching peroxisome, the cholesterol might be further oxidized or participate in bile acid synthesis in peroxisome. Cholesterol is also required for peroxisome lipid raft assembly and peroxisome biogenesis (van der Zand and Tabak, 2013; Woudenberg et al., 2010), and we estimated peroxisome contains ~5% of total cellular cholesterol (data not shown). Because disrupting LPMC decreases PM cholesterol level (Figure 2A) and impairs LDL-cholesterol reaching the ER (Figures 6E and 6F), it is likely that peroxisome may associate with other organelles and deliver cholesterol to them. This notion is further supported by the observation that cholesterol in lysosome increased by 20%–40% whereas cholesterol in peroxisome only decreased by ~2% after LPMC disruption in cells (Figure 6D). Alternatively, cholesterol transport via LPMC may be tightly coupled with cholesterol modification including oxidation and esterification. It is interesting to further study how cholesterol transportation is affected by cholesterol modification and vice versa. Besides cholesterol transfer, LPMC may regulate other functions of lysosome and peroxisome, such as autophagy, mTOR signaling, and peroxisome biogenesis.

Dramatic cholesterol accumulation was observed in X-ALD animal models and human patients' fibroblasts with mutations in different peroxisomal genes (Figure 7). Notably, the cholesterol accumulation (7-month-old) occurs long before the manifestation of the neurological phenotypes (20-month-old), suggesting intracellular cholesterol accumulation might be a potential mechanism causing X-ALD symptoms. It was also noted that although there was early onset of very long chain fatty

acid accumulation, relief of its accumulation did not significantly improve the disease symptoms (Prieto Tenreiro et al., 2013). On the other hand, it was well established that the accumulation of cholesterol in NPC disease patients is the cause of neuron death and neurological phenotypes. Mobilizing cholesterol by cyclodextrin constitutes a beneficial treatment for NPC patients (Liu et al., 2010). Therefore, the cholesterol trafficking blockage may underlie the pathological mechanism of peroxisome disorders, which could provide novel strategies for diagnosis and treatment of these diseases.

In summary, through functional genome-wide RNAi screen and hits analysis, we demonstrate the existence of lysosome-peroxisome membrane contacts mediated by Syt7-PI(4,5)P<sub>2</sub> binding, through which cholesterol is transported from lysosome to peroxisome. Peroxisomal disorders display significant intracellular cholesterol accumulation prior to neuronal symptoms. Together, this study suggests a central role of peroxisome in intracellular cholesterol trafficking and highlights the clinical relevance of cholesterol transport in peroxisomal disorders.

## EXPERIMENTAL PROCEDURES

Materials and plasmids, cell culture, growth assay, liposome flotation assay, and other procedures are described in the [Extended Experimental Procedures](#).

### shRNA Screen and Analysis

HeLa cells were infected with the MISSION LentiPlex human pooled shRNA library consists of over 75,000 shRNA constructs from the TRC collection targeting 15,000+ human genes. Infected cells were selected with puromycin (2 μg/ml) for 4 days. After five rounds of AmB selections ([Extended Experimental Procedures](#)), survived populations were collected, and shRNA inserts were amplified from genomic DNA by PCR. PCR products were sequenced by deep-sequencing. All the deep sequencing data were log<sub>10</sub> transformed and normalized to standard derivation from the screen-wide mean, which depicted as Z score [ $Z = (\text{gene's deep sequencing score} - \text{average deep sequencing score}) / \text{screen standard derivation}$ ]. Z score equal to 1.96 ( $p = 0.05$ ) was used as cut-off value to determine the screen hits. Genes with Z score over 1.96 ( $p < 0.05$ ) or targeted by five independent shRNAs were considered as screen hits.

### Organelle Co-Precipitation Assay

Triplicate samples for each treatment were homogenized in extraction buffer (5 mM MOPS [pH 7.65], with 0.25 M sucrose, 1 mM EDTA, 0.1% ethanol and protease inhibitors) and centrifuged at 1,000 × g for 10 min. Supernatants

## Figure 6. Transfer of <sup>3</sup>H-Cholesterol from Lysosome to Peroxisome

(A) Outline of the in vitro <sup>3</sup>H-cholesterol transfer assay.

(B) Ni Sepharoses bound-peroxisome was preincubated with anti-PI(4,5)P<sub>2</sub> or control IgG and then used for the in vitro <sup>3</sup>H-cholesterol transfer assay. Values are expressed as the percentage of <sup>3</sup>H-cholesterol in lysosome prior to reaction and presented as the mean ± SD of three independent repeats of experiments. \*\* $p < 0.01$ .

(C) Radiolabeled lysosomes were isolated from cells transfected with indicated siRNAs. Peroxisome was purified from wild-type cells and were then used for the in vitro <sup>3</sup>H-cholesterol transfer assay as in (A). Data are presented as the mean ± SD of three independent repeats of the experiments. \*\* $p < 0.01$ .

(D) HEK293T cells transfected with indicated siRNAs were depleted of cholesterol and then pulsed with <sup>3</sup>H-cholesteryl oleate-LDL for 3 hr. Then, lysosome and peroxisome were purified separately and the <sup>3</sup>H-cholesterol were measured. Values are expressed as percentage of control lysosome and presented as the mean ± SD of three independent experiments. \* $p < 0.05$ , \*\* $p < 0.01$ .

(E) HeLa cells transfected with indicated siRNAs were subjected to analysis of SREBP-2 cleavage. pSREBP2, precursor of SREBP2; nSREBP2, nuclear form of SREBP2; CHC, clathrin heavy chain. \*Indicates the nonspecific band.

(F) HeLa cells transfected with the indicated siRNAs were subjected to cholesterol esterification assay. TG, triacylglycerol. Quantification of cholesteryl [<sup>14</sup>C]-esters was analyzed by Image J. NS, not significant, \*\* $p < 0.01$ .

(G) A working mechanism of LDL-derived cholesterol transport out of lysosome.

See also [Figure S7](#).

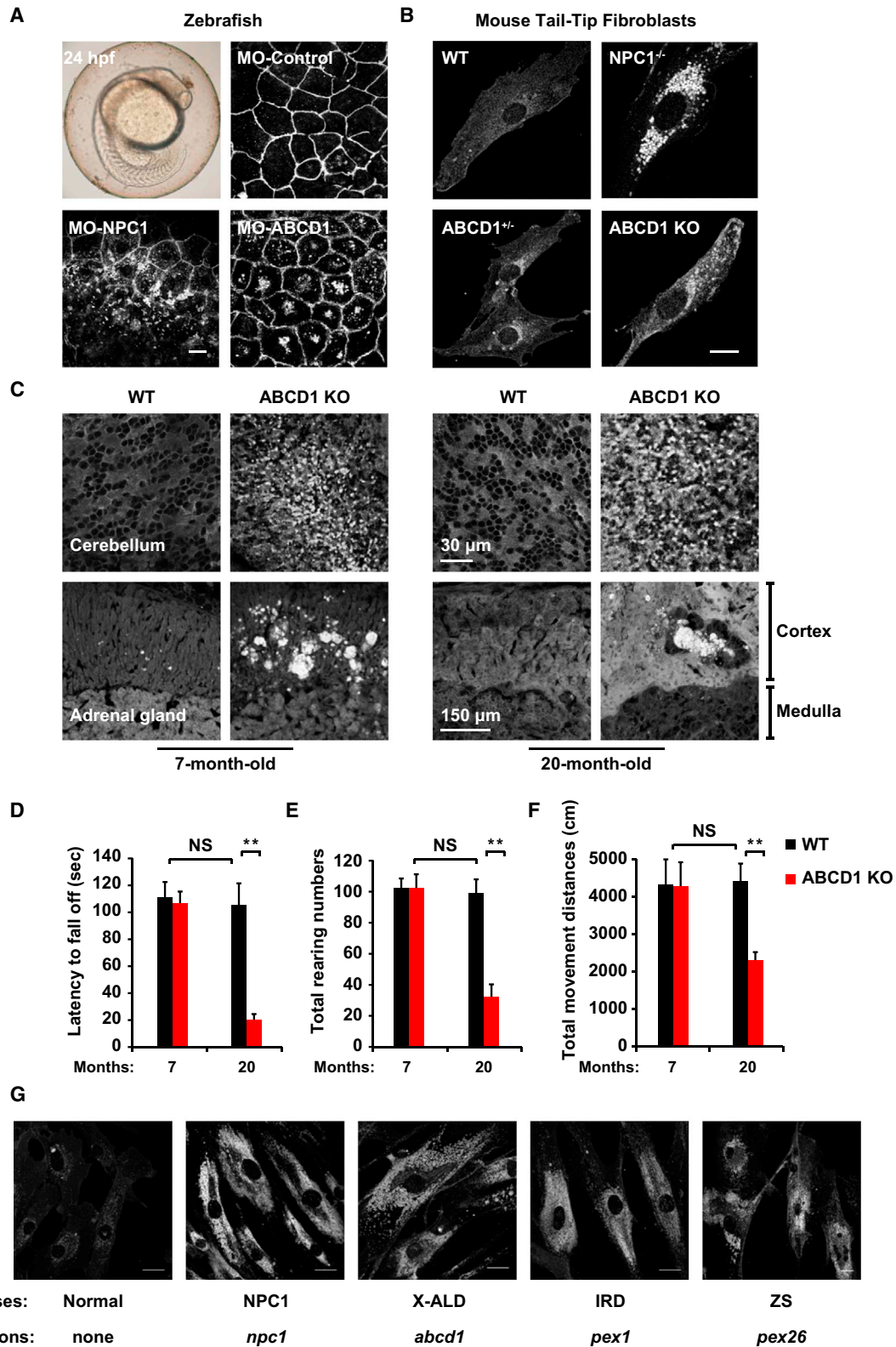


**Figure 7. Cholesterol Accumulation in Animals and Human Patients with Peroxisomal Disorders**

(A) Filipin staining of unesterified cholesterol in zebrafish embryos. Scale bar, 10 μm.

(B) Filipin staining of the tail-tip fibroblast cells from the mice at the age of 7 months (n = 4 per group). Scale bar, 10 μm.

(legend continued on next page)

were incubated with Ni Sepharoses at 4°C rotating for 2 hr. Beads were washed five times with extraction buffer. Then, 1  $\mu$ l Ni Sepharoses were mounted and analyzed by confocal microscope. Proteins bound to Sepharoses were eluted and subjected to western blot.

#### In Vitro Reconstitution Assay

EGFP-His<sub>6</sub>-SKL-labeled peroxisome and NPC1-FLAG-mCherry-labeled lysosome were first isolated by iodixanol density gradient centrifugation, respectively. The lysosome fractions were diluted with reconstitution buffer (250 mM sucrose, 1 mM DTT, 1 mM MgCl<sub>2</sub>, 50 mM KCl, and 20 mM HEPES [pH 7.2]), precipitated at 28,000  $\times$  g for 30 min and resuspended in reconstitution buffer. The peroxisome fractions were incubated with Ni Sepharoses, washed with reconstitution buffer plus 2 mM EGTA for four times, and then incubated with lysosome in the presence or absence of 1 mg/ml cytosol, 1 mM ATP, 1 mM GTP, and ATP-regenerating system (30 mM creatine phosphate, 0.05 mg/ml creatine kinase) at 37°C for 30 min. If needed, anti-PI(4,5)P<sub>2</sub> and Syt7-C2AB protein were applied 10 min at 4°C before the addition of ATP-regenerating system and cytosol. Ni Sepharoses were spun down, washed with reconstitution buffer, and subjected to microscopy and western blot.

#### In Vitro <sup>3</sup>H-Cholesterol Transfer Assay

Cells were incubated with 1  $\mu$ Ci/ml <sup>3</sup>H-cholesterol in growth medium overnight. The cells were then washed with PBS containing 0.2% BSA twice. The <sup>3</sup>H-cholesterol-labeled lysosome was isolated and its content of <sup>3</sup>H-cholesterol was measured using liquid scintillation. Peroxisome was purified from unlabeled cells by aforementioned method. The peroxisome and <sup>3</sup>H-cholesterol-labeled lysosome were subjected to in vitro reconstitution assay as described above. After incubation for different time durations at 37°C, the samples were spun down and lysosome was washed off by washing with reconstitution buffer plus 2 mM EGTA for four times. The <sup>3</sup>H-cholesterol on Ni Sepharoses bound-peroxisome was measured by liquid scintillation. The <sup>3</sup>H-cholesterol content in peroxisome was then normalized to the total input <sup>3</sup>H-cholesterol content of lysosome prior to reaction and was expressed as a percentage.

#### Measurement of LDL-Derived <sup>3</sup>H-Cholesterol in Lysosome and Peroxisome

After transfected with the indicated siRNAs, HEK293T cells were cultured in cholesterol-depleting medium for 16 hr and incubated with <sup>3</sup>H-cholesteryl oleate-LDL for 3 hr at 37°C. Then the cells were washed with PBS containing 0.2% BSA twice. Lysosome or peroxisome fractions were isolated by density gradient centrifugation separately and analyzed in a liquid scintillation counting.

#### Animals and Treatment

All animals were maintained and used in accordance with the guidelines of the Institutional Animal Care and Use Committee of the Shanghai Institutes for Biological Sciences. Mice were treated as described in the figure legends.

#### SUPPLEMENTAL INFORMATION

Supplemental Information includes Extended Experimental Procedures, seven figures, two tables, and two movies and can be found with this article online at <http://dx.doi.org/10.1016/j.cell.2015.02.019>.

#### AUTHOR CONTRIBUTIONS

B.-L.S. conceived the project. B.-B.C., Y.-C.L., W.Q., B.-L.L., and B.-L.S. designed the experiments. B.-B.C. and Y.-C.L. performed the main experiments and analyzed data. C.X. performed SREBP cleavage and cholesterol esterifi-

cation assays. X.D. and H.Y. contributed to human patients' cells study. J.W. performed murine NPC1-TAP purification and mass spectrometry. Experiments were assisted by contributions from H.-H.M. Manuscript was written by B.-B.C., Y.-C.L., W.Q., and B.-L.S. with input from all the other authors.

#### ACKNOWLEDGMENTS

We thank Yu-Xiu Qu, Jie Xu, and Jie Qin for technical assistance. We thank Dr. Dawei Zhang (University of Alberta) for measuring ABCD1 activity, Dr. Fei Sun (Institute of Biophysics, Chinese Academy of Sciences) for helping with EM, Dr. TY Chang (Dartmouth Medical School) for CT43 cells, and Dr. Xiangdong Fu (Wuhan University) for helpful discussion and critical reading the manuscript. This work was supported by the grants from the National Natural Science Foundation (NNSF) of China (31430044, 31230020, and 91413112), the Ministry of Science and Technology (MOST) of China (2011CB910900 and 2012CB524900), Shanghai Science and Technology Committee (13XD1404100) and the 10,000 Talents Plan. X.D. and H.Y. were supported by grant APP1041301 from the National Health and Medical Research Council (NHMRC), Australia. H.Y. is a Senior Research Fellow of the NHMRC.

Received: August 11, 2014

Revised: December 18, 2014

Accepted: February 3, 2015

Published: April 9, 2015

#### REFERENCES

- Andreoli, T.E. (1973). On the anatomy of amphotericin B-cholesterol pores in lipid bilayer membranes. *Kidney Int.* 4, 337–345.
- Andrews, N.W., and Chakrabarti, S. (2005). There's more to life than neurotransmission: the regulation of exocytosis by synaptotagmin VII. *Trends Cell Biol.* 15, 626–631.
- Brown, M.S., and Goldstein, J.L. (1986). A receptor-mediated pathway for cholesterol homeostasis. *Science* 232, 34–47.
- Brown, M.S., and Goldstein, J.L. (1997). The SREBP pathway: regulation of cholesterol metabolism by proteolysis of a membrane-bound transcription factor. *Cell* 89, 331–340.
- Carstea, E.D., Morris, J.A., Coleman, K.G., Loftus, S.K., Zhang, D., Cummings, C., Gu, J., Rosenfeld, M.A., Pavan, W.J., Krizman, D.B., et al. (1997). Niemann-Pick C1 disease gene: homology to mediators of cholesterol homeostasis. *Science* 277, 228–231.
- Chang, T.Y., Chang, C.C., and Cheng, D. (1997). Acyl-coenzyme A:cholesterol acyltransferase. *Annu. Rev. Biochem.* 66, 613–638.
- Chang, T.Y., Chang, C.C., Ohgami, N., and Yamauchi, Y. (2006). Cholesterol sensing, trafficking, and esterification. *Annu. Rev. Cell Dev. Biol.* 22, 129–157.
- Chen, Y.A., and Scheller, R.H. (2001). SNARE-mediated membrane fusion. *Nat. Rev. Mol. Cell Biol.* 2, 98–106.
- Conner, S.D., and Schmid, S.L. (2002). Identification of an adaptor-associated kinase, AAK1, as a regulator of clathrin-mediated endocytosis. *J. Cell Biol.* 156, 921–929.
- Desai, R.C., Vyas, B., Earles, C.A., Littleton, J.T., Kowalchuck, J.A., Martin, T.F., and Chapman, E.R. (2000). The C2B domain of synaptotagmin is a Ca(2+)-sensing module essential for exocytosis. *J. Cell Biol.* 150, 1125–1136.
- Du, X., Kumar, J., Ferguson, C., Schulz, T.A., Ong, Y.S., Hong, W., Prinz, W.A., Parton, R.G., Brown, A.J., and Yang, H. (2011). A role for oxysterol-binding protein-related protein 5 in endosomal cholesterol trafficking. *J. Cell Biol.* 192, 121–135.

(C) Filipin staining of cerebellum and adrenal gland from different genotypes of mice.

(D) Motor performance of mice in a rotarod test.

(E) Quantification of rearing behavior of mice submitted to the open field test (n = 4 per group).

(F) The total distance moved within the open field arena (40 cm  $\times$  40 cm) was assessed over 15 min (n = 4 per group).

(G) Filipin staining of the cultured fibroblasts from human patients with indicated diseases. Scale bar, 25  $\mu$ m.

- Forss-Petter, S., Werner, H., Berger, J., Lassmann, H., Molzer, B., Schwab, M.H., Bernheimer, H., Zimmermann, F., and Nave, K.A. (1997). Targeted inactivation of the X-linked adrenoleukodystrophy gene in mice. *J. Neurosci. Res.* *50*, 829–843.
- Fukuda, M., and Mikoshiba, K. (2001). Mechanism of the calcium-dependent multimerization of synaptotagmin VII mediated by its first and second C2 domains. *J. Biol. Chem.* *276*, 27670–27676.
- Goldstein, J.L., DeBose-Boyd, R.A., and Brown, M.S. (2006). Protein sensors for membrane sterols. *Cell* *124*, 35–46.
- Hardeman, D., Versantvoort, C., van den Brink, J.M., and van den Bosch, H. (1990). Studies on peroxisomal membranes. *Biochim. Biophys. Acta* *1027*, 149–154.
- Ishibashi, S., Schwarz, M., Frykman, P.K., Herz, J., and Russell, D.W. (1996). Disruption of cholesterol 7 $\alpha$ -hydroxylase gene in mice. I. Postnatal lethality reversed by bile acid and vitamin supplementation. *J. Biol. Chem.* *271*, 18017–18023.
- Jeynov, B., Lay, D., Schmidt, F., Tahirovic, S., and Just, W.W. (2006). Phosphoinositide synthesis and degradation in isolated rat liver peroxisomes. *FEBS Lett.* *580*, 5917–5924.
- Kapitein, L.C., Schlager, M.A., Kuijpers, M., Wulf, P.S., van Spronsen, M., MacKintosh, F.C., and Hoogenraad, C.C. (2010). Mixed microtubules steer dynein-driven cargo transport into dendrites. *Curr. Biol.* *20*, 290–299.
- Kwon, H.J., Abi-Mosleh, L., Wang, M.L., Deisenhofer, J., Goldstein, J.L., Brown, M.S., and Infante, R.E. (2009). Structure of N-terminal domain of NPC1 reveals distinct subdomains for binding and transfer of cholesterol. *Cell* *137*, 1213–1224.
- Lange, Y., Ye, J., Rigney, M., and Steck, T.L. (1999). Regulation of endoplasmic reticulum cholesterol by plasma membrane cholesterol. *J. Lipid Res.* *40*, 2264–2270.
- Liscum, L., and Faust, J.R. (1989). The intracellular transport of low density lipoprotein-derived cholesterol is inhibited in Chinese hamster ovary cells cultured with 3- $\beta$ -[2-(diethylamino)ethoxy]androst-5-en-17-one. *J. Biol. Chem.* *264*, 11796–11806.
- Liscum, L., and Munn, N.J. (1999). Intracellular cholesterol transport. *Biochim. Biophys. Acta* *1438*, 19–37.
- Liu, B., Ramirez, C.M., Miller, A.M., Repa, J.J., Turley, S.D., and Dietschy, J.M. (2010). Cyclodextrin overcomes the transport defect in nearly every organ of NPC1 mice leading to excretion of sequestered cholesterol as bile acid. *J. Lipid Res.* *51*, 933–944.
- Matsumoto, N., Tamura, S., and Fujiki, Y. (2003). The pathogenic peroxin Pex26p recruits the Pex1p-Pex6p AAA ATPase complexes to peroxisomes. *Nat. Cell Biol.* *5*, 454–460.
- Moser, H.W., Raymond, G.V., and Dubey, P. (2005). Adrenoleukodystrophy: new approaches to a neurodegenerative disease. *J. Am. Med. Assoc.* *294*, 3131–3134.
- Prieto Tenreiro, A., Penacho Lazaro, M.A., Andres Celda, R., Fernandez Fernandez, M., Gonzalez Mateo, C., and Diez Hernandez, A. (2013). Dietary treatment for X-linked adrenoleukodystrophy: is “Lorenzo’s oil” useful? *Endocrinologia y nutricion* *60*, 37–39.
- Rosenbaum, A.I., Zhang, G., Warren, J.D., and Maxfield, F.R. (2010). Endocytosis of beta-cyclodextrins is responsible for cholesterol reduction in Niemann-Pick type C mutant cells. *Proc. Natl. Acad. Sci. USA* *107*, 5477–5482.
- Sleat, D.E., Wiseman, J.A., El-Banna, M., Price, S.M., Verot, L., Shen, M.M., Tint, G.S., Vanier, M.T., Walkley, S.U., and Lobel, P. (2004). Genetic evidence for nonredundant functional cooperativity between NPC1 and NPC2 in lipid transport. *Proc. Natl. Acad. Sci. USA* *101*, 5886–5891.
- Troffer-Charlier, N., Doerflinger, N., Metzger, E., Fouquet, F., Mandel, J.L., and Aubourg, P. (1998). Mirror expression of adrenoleukodystrophy and adrenoleukodystrophy related genes in mouse tissues and human cell lines. *Eur. J. Cell Biol.* *75*, 254–264.
- Urano, Y., Watanabe, H., Murphy, S.R., Shibuya, Y., Geng, Y., Peden, A.A., Chang, C.C., and Chang, T.Y. (2008). Transport of LDL-derived cholesterol from the NPC1 compartment to the ER involves the trans-Golgi network and the SNARE protein complex. *Proc. Natl. Acad. Sci. USA* *105*, 16513–16518.
- van der Zand, A., and Tabak, H.F. (2013). Peroxisomes: offshoots of the ER. *Curr. Opin. Cell Biol.* *25*, 449–454.
- Vance, J.E., and Vance, D.E. (1990). Lipoprotein assembly and secretion by hepatocytes. *Annu. Rev. Nutr.* *10*, 337–356.
- Weber, T., Zemelman, B.V., McNew, J.A., Westermann, B., Gmachl, M., Parlati, F., Söllner, T.H., and Rothman, J.E. (1998). SNAREpins: minimal machinery for membrane fusion. *Cell* *92*, 759–772.
- Woudenberg, J., Rembacz, K.P., Hoekstra, M., Pellicoro, A., van den Heuvel, F.A., Heegsma, J., van Ijendoorn, S.C., Holzinger, A., Imanaka, T., Moshage, H., and Faber, K.N. (2010). Lipid rafts are essential for peroxisome biogenesis in HepG2 cells. *Hepatology* *52*, 623–633.